The Tropospheric Land–Sea Warming Contrast as the Driver of Tropical Sea Level Pressure Changes

TOBIAS BAYR

Helmholtz Centre for Ocean Research Kiel (GEOMAR), Kiel, Germany

DIETMAR DOMMENGET

School of Mathematical Sciences, Monash University, Clayton, Victoria, Australia

(Manuscript received 15 December 2011, in final form 19 July 2012)

ABSTRACT

This article addresses the causes of the large-scale tropical sea level pressure (SLP) changes during climate change. The analysis presented here is based on model simulations, observed trends, and the seasonal cycle. In all three cases the regional changes of tropospheric temperature (T_{tropos}) and SLP are strongly related to each other [considerably more strongly than (sea) surface temperature and SLP]. This relationship basically follows the Bjerknes circulation theorem, with relatively low regional SLP where there is relatively high T_{tropos} and vice versa. A simple physical model suggests a tropical SLP response to horizontally inhomogeneous warming in the tropical T_{tropos}, with a sensitivity coefficient of about -1.7 hPa K^{-1}. This relationship explains a large fraction of observed and predicted changes in the tropical SLP.

It is shown that in climate change model simulations the tropospheric land–sea warming contrast is the most significant structure in the regional T_{tropos} changes relative to the tropical mean changes. Since the land–sea warming contrast exists in the absence of any atmospheric circulation changes, it can be argued that the large-scale response of tropical SLP changes is to first order a response to the tropical land–sea warming contrast. Furthermore, as the land–sea warming contrast is mostly moisture dependent, the models predict a stronger warming and decreasing SLP in the drier regions from South America to Africa and a weaker warming and increasing SLP over the wetter Indo-Pacific warm pool region. This suggests an increase in the potential for deep convection conditions over the Atlantic sector and a decrease over the Indo-Pacific warm pool region in the future.

1. Introduction

The Fourth Assessment Report of the Intergovernmental Panel on Climate Change (IPCC) predicts a substantial global warming with a well-defined three-dimensional spatial pattern in atmospheric temperatures for future anthropogenic climate change. How the tropical sea level pressure (SLP) and atmospheric circulation change in response to these atmospheric temperature changes is the focus of this study.

The atmospheric temperature response to increasing greenhouse gas concentrations in the tropics has two important large-scale features: a vertical increase in warming of the troposphere and a land–sea warming contrast. The vertical increase in warming in the tropical troposphere is associated with the enhanced hydrological cycle (Held 1993; Held and Soden 2006) and is accompanied by a weakening of the large-scale tropical circulation (Vecchi et al. 2006; Vecchi and Soden 2007; Vecchi et al. 2008). The second feature, which is not restricted to the tropical regions, is the marked land–sea contrast of surface and low-level warming [i.e., a (stronger) heating over land relative to the oceans]. This is not just a transient effect caused by different heat capacities of land and oceans; rather, it is due to differences in feedbacks related to the available moisture (Sutton et al. 2007; Joshi et al. 2008; Dommenget 2009).

How land–sea contrast is generated is illustrated in Joshi et al. (2008): Above a certain level in the middle troposphere the warming is more or less horizontally uniform due to a strong mixing of these air masses (see also

Corresponding author address: Tobias Bayr, Helmholtz Centre for Ocean Research Kiel (GEOMAR), Düsternbrooker Weg 20, 24105 Kiel, Germany.
E-mail: tbayr@geomar.de

DOI: 10.1175/JCLI-D-11-00731.1

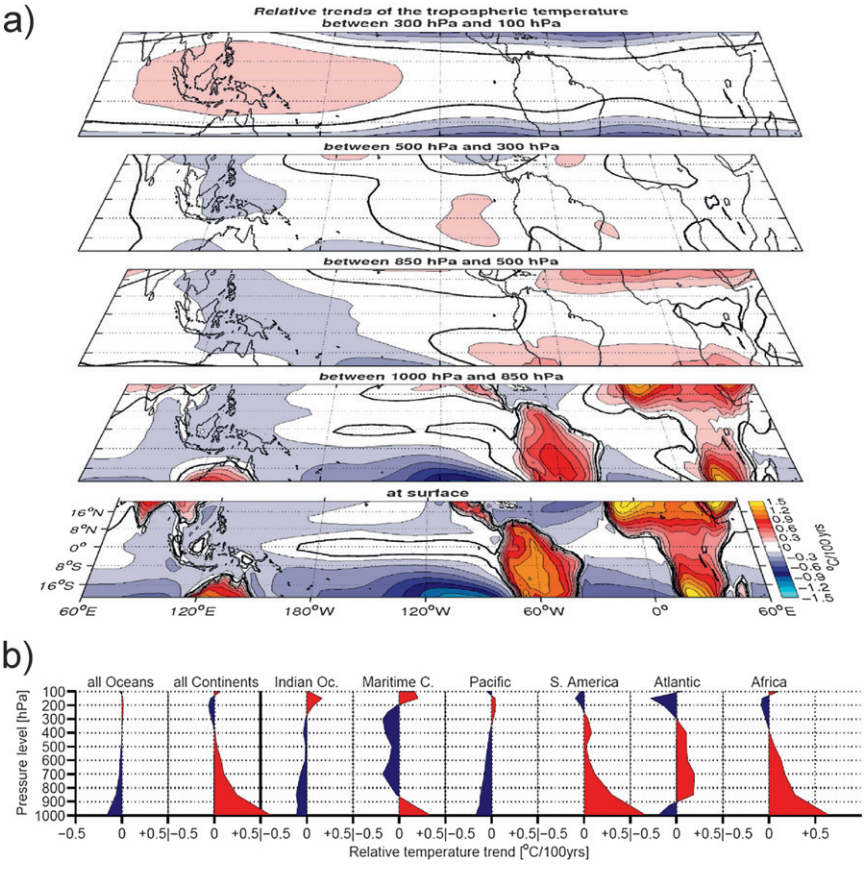

FIG. 1. (a) Linear trend of the IPCC multimodel ensemble for the period 1970–2099 for tropospheric temperature at surface and for layers 1000–850, 850–500, 500–300, and 300–100 hPa, with area mean trend of 2.4°, 2.6°, 3.0°, 4.2°, and 4.6°C (100 yr)$^{-1}$ (from bottom to top) removed. (b) As in (a), but here the vertical profile averaged over the named oceans and continents between 23°S and 23°N.

Fig. 1a, upper levels). Below this level, local feedbacks dominate the lapse rate and the warming. Because of more available latent heat the lapse rate is lower where the moisture content is higher and vice versa, with the dry adiabatic lapse rate as upper boundary. Thus, starting at the same temperature in the middle troposphere and following a moisture dependent adiabat, we yield a higher surface temperature at drier air columns and lower surface temperature at wetter air columns. Available moisture is limited over land, so that we get in general a stronger warming over land than over ocean, and thus a land–sea warming contrast. Thus, the terminology ''land–sea contrast'' can be somewhat misleading because it is mostly an ''available moisture contrast.''

Important aspects of land–sea warming contrast are shown in Fig. 1a. In the vertical it is most pronounced near the surface and in the horizontal it is strongest over the arid subtropical landmasses. In the layer from 850 to 500 hPa the dry trade wind inversions over the east Atlantic and east Pacific warm nearly as strongly as the dry air over the subtropical landmasses. The humid Maritime Continent has only a weak land–sea contrast at surface and no land–sea contrast in the lower troposphere. These two features become clearer in Fig. 1b: The Maritime Continent cools above the lowest levels (more oceanlike) and the Atlantic warms above the lowest levels (more landlike). The upper boundary of the land–sea warming contrast varies over the individual oceans and continent [in agreement with Joshi et al. (2008)], while in the tropical-wide perspective it is at the 400-hPa level (Fig. 1b). In summary, it is quite obvious in this figure that horizontal differences in the warming of each tropospheric level relative to the level's mean warming are highest in the lower levels, which are most strongly affected by the land–sea warming contrast. Since horizontal temperature gradients are one of the main drivers of the longitudinal atmospheric circulation

cells, it seems plausible that the land–sea warming contrast could be an important driver of tropical circulation and SLP changes. For example Bala et al. (2011) show that an artificial land–sea warming contrast due to geoengineering enhances the uplift and decreases the SLP over tropical landmasses.

In general there is an important contrary relationship between temperature and SLP. This can be observed in monsoon circulation and land–sea breeze and is described by the Bjerknes circulation theorem: Heating at one place and cooling at the other will induce a nearly direct circulation, with rising air and low SLP at the heat source and sinking air and high SLP at the heat sink (e.g., Bjerknes et al. 1898; Gill 1980; Thorpe et al. 2003), assuming that in the tropics the Coriolis force can be neglected. On regional scales previous studies (e.g., Hu et al. 2000) found that this relationship can explain the intensification of the Asian monsoonal circulation by the land–sea warming contrast.

We can now do a first simple thought experiment: We know that there are the three relatively warm places in the tropics (Indo-Pacific warm pool region, South America, and Africa) where the main deep convection takes place and SLP is low (Krueger and Winston 1974). We also know that in climate change projections due to the land–sea warming contrast two of the three warm places (Africa and South America) warm more strongly than the third (Indo-Pacific warm pool region; see Fig. 1) because highly available moisture reduces the warming there. Having the Bjerknes circulation theorem in mind, we would expect from this thought experiment that on large scales the SLP will increase over the warm pool region and decrease over Africa and South America, if the land–sea warming contrast is the dominant feature in the SLP trends.

In recent years the tropical SLP response in a warmer climate has often been discussed in the context of the weakening of the tropical circulations over the Pacific region, and thus also on a more regional than global scale. Since the land–sea warming contrast acts on a global scale, the question arises as to whether the large-scale SLP response in the tropics can be explained with the land–sea warming contrast.

To describe this relationship between temperature and SLP as precisely as possible, the temperature information of the atmosphere and not only of the surface is important, as indicated by the integration along the circulation path in the Bjerknes circulation theorem and stated in Flohn (1975). Further, considering only changes in surface temperature neglects the potentially important effects of the land–sea warming contrast on the troposphere. As we will see in the results section, the SLP response in a warmer climate can be described considerably better if the temperature change over the full tropospheric circulation domain is considered, from surface to tropopause.

The focus of this study is to investigate the link between tropospheric temperature T_{tropos} and SLP changes in climate model simulations of future climate change simulations and in observations. We aim to present a simple physical model that can explain a large fraction of the large-scale response of the tropical SLP in a warming climate. The paper is organized as follows: Section 2 gives an overview of the data used in this study. This is followed by the first analysis in section 3, in which we investigate the relation between T_{tropos} and SLP in the mean seasonal cycle to establish the link between T_{tropos} and SLP. In section 4 a simple physical model for the tropical SLP response is introduced that quantifies the linear relation between T_{tropos} and SLP. The T_{tropos} and SLP trends of a climate change multimodel ensemble are examined in sections 5 and 6. The model simulation analysis is complemented by an idealized land–sea contrast experiment in section 7 and the trends in observations are investigated in section 8. We conclude our analysis with a summary and discussion in section 9.

2. Data

Observed atmospheric temperatures and SLP are taken from the interim European Centre for Medium-Range Weather Forecasts (ECMWF) Re-Analysis (ERA-Interim) data (Simmons et al. 2007) for the available period from 1989 to 2010. Over this period, the tropical temperature trends are in good agreement with satellite observations (Bengtsson and Hodges 2009). We assume that the reanalysis products are the best estimates of observed tropospheric temperatures for this study, particularly because of the lack of sufficient coverage of ''real'' observations for the vertical air temperature profile.

The future climate change simulation data used are from 23 coupled model simulations of phase 3 of the Climate Model Intercomparison Project 3 (CMIP3; Meehl et al. 2007b). We took all simulations from the CMIP3 database that have atmospheric temperature and SLP for the IPCC 20C and A1B scenario available, interpolated all data on a regular $2.5° \times 2.5°$ grid, and calculated a multimodel ensemble mean with one ensemble member from each model. Missing atmospheric temperature values due to topography are interpolated from the levels above, following a moist adiabatic temperature profile.

Additionally we analyzed a set of sensitivity experiments with the ECHAM5 atmospheric general circulation model (Roeckner et al. 2003) in T31 horizontal

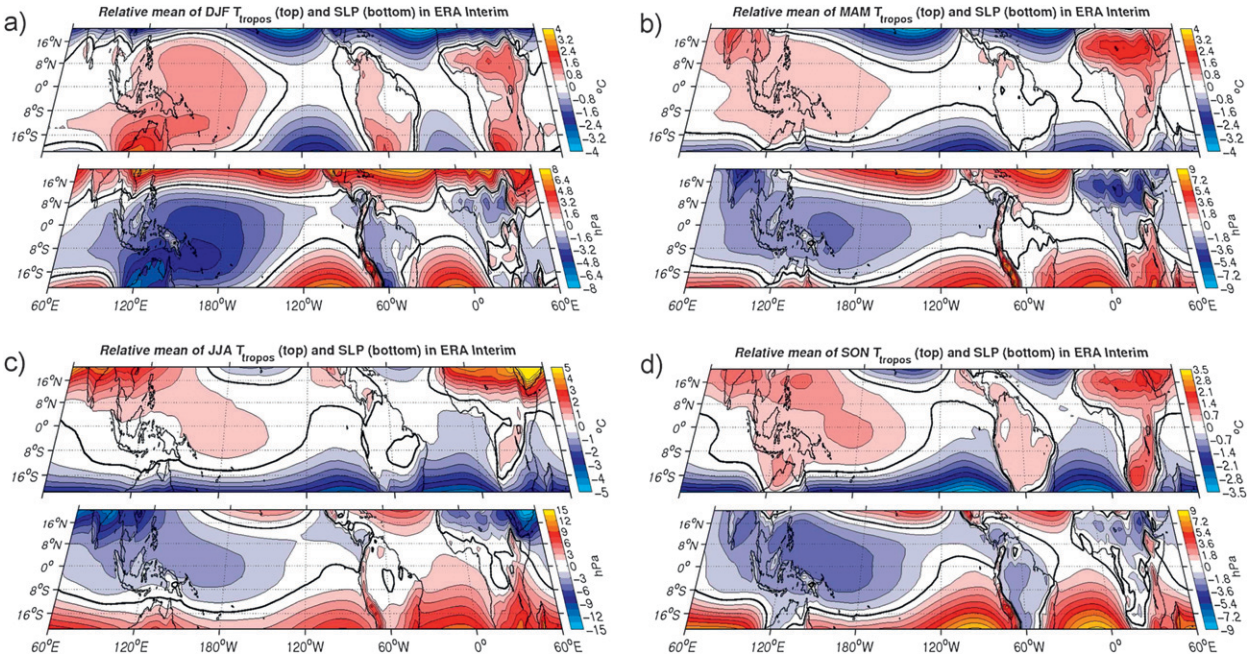

FIG. 2. Seasonal mean (top) T_{tropos} and (bottom) SLP in ERA-Interim relative to the tropics area total mean in (a) December–February (DJF; −10.0°C, 1011.8 hPa, −0.85) (b) March–May (MAM; −9.6°C, 1011.6 hPa, −0.87), (c) June–August (JJA; −9.9°C, 1012.7 hPa, −0.89), and (d) September–November (SON; −9.9°C, 1012.1 hPa, −0.87); values in brackets are the subtracted area mean for T_{tropos}, SLP, and the pattern correlation between the two patterns, respectively.

resolution (3.75° × 3.75°) coupled to a single column mixed layer ocean, as described in Dommenget (2009). We analyzed two 50-yr-long sensitivity experiments in which the land surface temperatures with +1-K and −1-K differences from a reference climatology are prescribed; see Dommenget (2009) for details.

For all following analyses we defined the tropospheric temperature, T_{tropos}, as the vertical average of mass weighted air temperature from 1000 to 100 hPa (i.e., approximately the entire troposphere). The tropics are defined as the region from 23°N to 23°S.

3. The seasonal cycle of tropical SLP and T_{tropos}

As a starting point for this study, we analyze the observed seasonal changes in tropospheric temperatures and SLP, as it provides a zero-order estimate of the tropical circulation response to changes in tropospheric temperatures or to external forcing (incoming solar radiation in this case) in general. In Figs. 2a–d we compare the seasonal mean T_{tropos} relative to the tropical total mean T_{tropos} with the seasonal mean SLP relative to the tropical total mean SLP. We can first of all note that the tropics have three regions of relative warm T_{tropos} over Africa, South America, and the Indo-Pacific warm pool region (including Australia), which are also called the three main ''heat sources,'' where the main deep convection takes place (Krueger and Winston 1974). These warm regions are separated by the cooler eastern Pacific and Atlantic and cooler regions toward higher latitudes. Following the seasonal cycle these regions shift mostly in north–south directions. More importantly in the context of this study, we can see that the patterns of relative T_{tropos} and SLP in all four seasons are highly anticorrelated with each other (Figs. 2a–d): The three main heat sources in the tropics coincide with the regions of lowest SLP (Matsuno 1966), as expected from the Bjerknes circulation theorem. The net mass exchange with the extratropics from season to season is small (despite the flow from summer to winter hemisphere), so that air masses redistribute mainly within the tropical band.

Another way of illustrating the strong relationship between relative T_{tropos} and relative SLP is to regress all four seasonal mean relative T_{tropos} values against the relative SLP for all grid points, as shown in Fig. 3. The distribution indicates a clear linear relationship between relative T_{tropos} and relative SLP consistent with the above discussion. As a first measure of the relation, we obtain from a linear regression a −2.4-hPa change in SLP per 1-K warming in T_{tropos} in the seasonal cycle, which can explain 76% ($R^2 = 0.76$) of the SLP seasonal means with the T_{tropos} seasonal means.

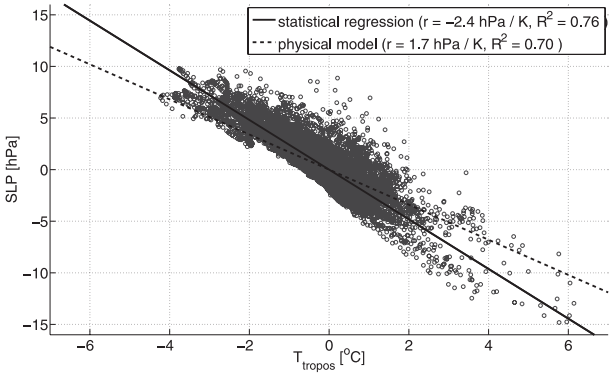

FIG. 3. Regression between relative T_{tropos} and SLP pattern from Figs. 2a–d for all four seasons together.

4. A simple physical model for tropical SLP response to changes in T_{tropos}

From simple physical considerations we can build a physical model to estimate the linear relationship between relative T_{tropos} and relative SLP in the tropics. Figure 4 illustrates how a regionally different warming of T_{tropos} can cause a mass redistribution and therefore a change in SLP. With regard to the Bjerknes circulation theorem we propose the following mechanism behind the simple model: We consider initially two air columns with the same temperature and pressure (Fig. 4a). Warming the left column will expand the air, and cooling the right will contract the air (Fig. 4b). In the real world the Bjerknes circulation tries to balance the temperature differences and induces a lateral mass flow between the warmer and the colder air column and causes an SLP change. In our physical model we assume that the heights of the two columns are balanced at the end again (Fig. 4c). As in a hydrostatic framework the pressure is just the weight of the mass above. We start in our simple model with the hydrostatic equation:

$$dp = -\rho g\, dh, \tag{1}$$

with pressure p, density ρ, gravity constant g, and air column height h. With

$$dh = \frac{h}{T}\, dT \tag{2}$$

we can calculate the isobaric thermal expansion of the air column using the ideal gas law, with temperature T. To balance the heights of the two columns at the end, half of the height difference is moved from the warmer to the colder air volume. So with both equations we obtain for the SLP change in dependency of the temperature change

$$\frac{dp}{dT} = 0.5\rho g \frac{h}{T}. \tag{3}$$

Our model assumes lateral mass flow so that the pressure changes of many thin air volumes integrated vertically over the whole column are the same as the mass flow of one 900-hPa-thick column. This allows us

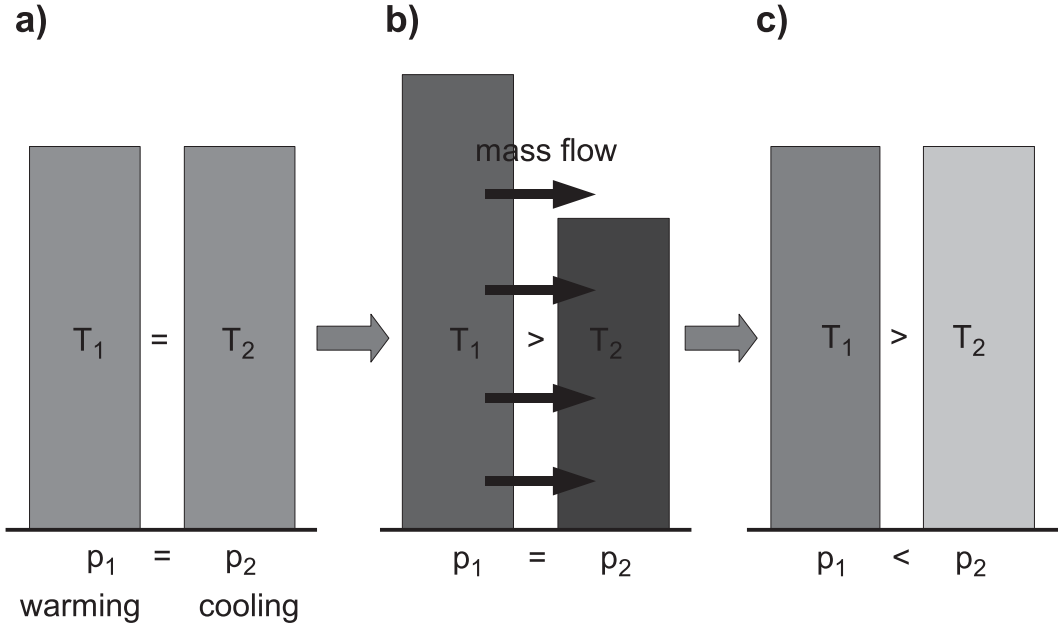

FIG. 4. Schematic of the physical model (for details see text).

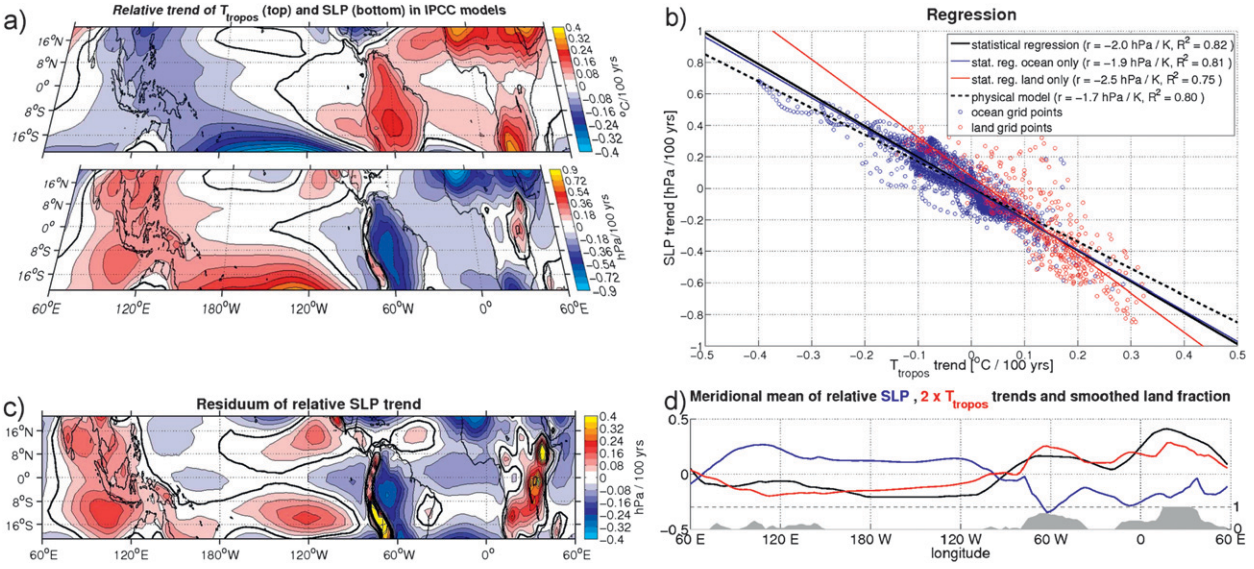

FIG. 5. (a) As in Fig. 2, but for linear trend of the IPCC multimodel ensemble for the period 1970–2099; area mean trend removed [3.6°C (100 yr)$^{-1}$ for T_{tropos} and 0.05 hPa (100 yr)$^{-1}$ for SLP]. (b) Regression of the two-trend pattern in (a). (c) Residuum of relative SLP trend after applying the physical model to multimodel ensemble data. (d) Meridional mean of the two-trend pattern in (a) and land fraction of the area between 23°S and 23°N in black, smoothed with a running mean of 60° and mean value subtracted; the gray filled area is the unsmoothed meridional mean of land fraction, with the *y* axis on the right.

to use the hydrostatic equation. From ERA-Interim we obtain for the mean tropospheric density $\rho = 0.562$ kg m^{-3}, troposphere height $h = 16.5$ km, and tropospheric temperature $T = 263.6$ K, so that we yield a pressure change of -1.7 hPa at the surface per 1-K warming of the tropospheric air column above. This value is close to the statistical regression coefficient found in Fig. 3, indicating that the simple model describes a significant part of the SLP response to T_{tropos}. However, there is also a statistically significant deviation from the observed relationship, indicating that the model is not a complete match.

There are four assumptions for this model. First, the model only considers relative (inhomogeneous) changes in T_{tropos} and SLP, which means a mass redistribution only inside the tropics for SLP and a local heating relative to the tropical average for T_{tropos}. Thus, the area mean is removed from SLP and T_{tropos} (as in Figs. 2a–d) before applying the simple model. A homogenous warming of T_{tropos} has no effect on SLP, as it would not induce any regional SLP changes (mass redistribution inside the tropics). The seasonal changes of the absolute values of T_{tropos} and SLP (Figs. 2a–d) are an order of magnitude smaller than the regional differences within one season. Thus, the inhomogeneous variations are much more pronounced than the homogeneous. With respect to the seasonal cycle, we can explain 70% of the SLP changes by the changes in T_{tropos} (Fig. 3), which is only 6% less than in the statistical regression.

Second, it is assumed that the T_{tropos} changes are given and independent of SLP changes. Thus, SLP changes are assumed to be a response to T_{tropos}, but do not cause changes in T_{tropos}. This is a simplification, as changes in SLP or more generally in the atmospheric circulation will cause changes in T_{tropos}. However, the main feature in T_{tropos} change is the land–sea warming contrast (cf. Figs. 1a and 5a, top) due to processes and feedbacks that do not involve atmospheric circulation changes (Joshi et al. 2008; Dommenget and Flöter 2011). Indeed, the tropical land–sea warming contrast can be reproduced very well in a global energy balance climate model that does not simulate atmospheric circulation changes (Dommenget and Flöter 2011). Thus, atmospheric circulation feedbacks can be considered as a secondary effect.

Third, the model does not consider that vertical column extent varies with topography. Since we interpolated all columns to sea level height, we implicitly assumed that this topographic effect is of secondary order.

Fourth, a pressure level exists in which we have nearly no horizontal gradients in the geopotential height change, so that the mass has to redistribute below this level. This is most valid at the tropopause layer, which is in the tropics roughly at the 100-hPa level (not shown).

5. Projected trends in the multimodel ensemble

Having established the fidelity of our simple model to describe the tropical SLP response to T_{tropos} changes

over the seasonal cycle, we can now look at the multimodel ensemble mean trends of tropical climate change simulations for the period 1970–2099. First, we can note that the SLP trend averaged over the entire tropics is 0.05 hPa (100 yr)$^{-1}$ and is an order of magnitude smaller than the relative trends [about 0.22 hPa (100 yr)$^{-1}$; spatial standard deviation of Fig. 5a, bottom], indicating that mass flow in or out of the tropics is small compared to the tropical internal changes. Thus, relative SLP changes in the tropics mark the main signal of tropical SLP changes. In contrast the T_{tropos} absolute trend [3.6°C (100 yr)$^{-1}$] is about an order of magnitude larger than the relative trends [up to ±0.4°C (100 yr)$^{-1}$].

Figure 5a shows the linear trend patterns in relative T_{tropos} and relative SLP for the period 1970–2099. Relative to the tropical mean warming, the troposphere over Africa and South America warms most (Fig. 5a, top). A second strong relative warming appears in the very dry trade wind inversions over the eastern parts of the subtropical Atlantic and South Pacific. In agreement with the available moisture dependence of the land–sea warming contrast, the models predict a relative cooling over the Indo-Pacific warm pool region. Thus, the land–sea contrast of surface and midlevel warming dominates the T_{tropos} trend pattern. The ensemble mean relative trend of tropical SLP (Fig. 5a, bottom) is mostly opposite to the T_{tropos} trend pattern. This roughly zonal structure shows a mass redistribution from the Atlantic region to the warm pool region, and exhibits, as in the T_{tropos} trend pattern, only small seasonal variations (not shown). Again, the strong linear relationship between relative T_{tropos} and relative SLP trends can be illustrated by a scatterplot (see Fig. 5b). The linear regression coefficient between all T_{tropos} and SLP trend points is −2.0 hPa K^{-1}, which is a bit larger in magnitude than the physical model value of −1.7 hPa K^{-1}.

In this scatterplot the ocean grid points are colored in blue and the land grid points in red. Most ocean grid points have a negative trend in T_{tropos} and positive trend in SLP, and vice versa for the land grid points. Thus, the relatively clear separation of land and ocean grid points in this point cloud illustrates again that the land–sea warming contrast is the major driver for the tropical SLP changes. However, even if we look at the relation between T_{tropos} and SLP for ocean or land points only, we find the same basic linear relationship. The linear regression coefficient and explained variance (R^2) values are similar for all ocean points, with a bit stronger regression coefficient but smaller R^2 value for all land points. This mainly suggests that the link between T_{tropos} and SLP exists also on the smaller scales (e.g., within the continental regions) and is not just between land and ocean contrast, underlining the general relevance of Bjerknes circulation theorem in the tropics.

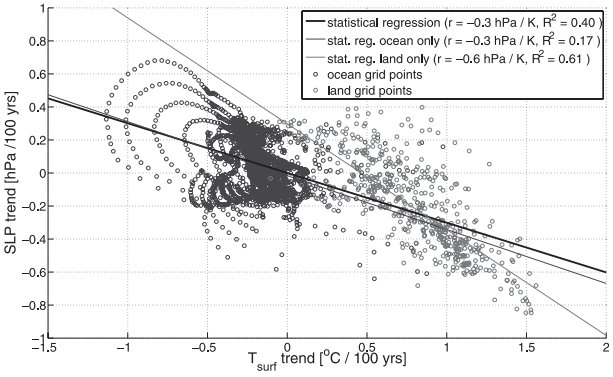

FIG. 6. Linear regression between relative trends of T_{surf} (Fig. 1a, bottom) and SLP (Fig. 5a, bottom) in the IPCC multimodel ensemble for the period 1970– 2099.

It is important to note here that the relationship of the surface temperature (T_{surf}) or SST and the SLP is not as clear as the relationship between T_{tropos} and SLP, because there are some significant changes in the relative warmings at different levels (see Fig. 1b). At the near surface (below 850 hPa) the local land–sea distribution is dominating the warming contrast, but at the midlevels from 850 to 400 hPa the large-scale land–sea distribution is more important. In total we get therefore T_{tropos} trends with a large-scale hemispheric warming contrast between the hemisphere with more land (South America to Africa) and the hemisphere with mostly ocean (Indo-Pacific).

To underline the importance of considering the whole tropospheric warming instead of just the surface warming, we analyze the relation between T_{surf} or SST and SLP. In Fig. 6 the regression of T_{surf} (black line) and SST (dark gray line) shows a much weaker regression coefficient of 0.3 hPa K^{-1}, which can be explained by the stronger gradients at the surface than in T_{tropos}. But more important in the comparison is that with $R^2 = 0.82$ T_{tropos} can explain twice as much of the SLP trends as T_{surf} with $R^2 = 0.40$ and nearly 5 times as much as SST with $R^2 = 0.17$ in a linear fit. This figure in comparison with Fig. 5b confirms as stated in Flohn (1975) that tropospheric temperature can describe the SLP response in a warming climate considerably better than (sea) surface temperature.

With the T_{tropos} trends our physical model can explain with 80% only 2% less of the SLP trends as the statistical regression. The residual SLP trends of the physical model are shown in Fig. 5c (note the different color bar): Much of the trend signal is gone, highlighting that the model can explain a large part of the SLP trends, and the

residuum trend no longer shows the large-scale mass redistribution but more local trends.

The contrary relationship between relative T_{tropos} and SLP trends can also be seen very nicely in the meridional mean of the two-trend pattern (Fig. 5d), with a correlation of -0.94 between the red and the blue curve. The dependency of the responses to the land warming shows up in comparison with the meridional mean of the tropical land fraction (black line in Fig. 5d), which is smoothed with a running mean of 60° and the mean value subtracted (correlation of 0.90 with T_{tropos} and -0.84 with SLP) or in comparison with the unsmoothed tropical land fraction (gray shaded area in Fig. 5d, correlation of 0.75 with T_{tropos} and -0.58 with SLP), only disagreeing slightly over the warm pool region. But this can be explained by the small size of the islands of the Maritime Continent, which leads to a more oceanlike cooling in the layers above the surface due to the close proximity of the oceans for all land points in coarse-resolution models (Fig. 1b).

6. Projected trends in the individual CMIP3 models

The response of individual IPCC models in the A1B scenario can be quite different from model to model. It is therefore instructive to discuss the distribution in the relationship between the relative T_{tropos} and SLP trends for all the IPCC models. Table 1 lists some important values for all the individual IPCC models. The absolute trends of tropical T_{tropos} have values between 2.2° and 5.5°C (100 yr)$^{-1}$, on average 3.6°C (100 yr)$^{-1}$, nearly the same spread and magnitude as the trends of the global mean surface temperature (Meehl et al. 2007a).

Notable are the global mean SLP trends in the models, which suggest some unphysical trends that will have no impact on the atmospheric circulation. For most models the trends of the tropical SLP are very similar to the global mean trends (correlation of Table 1's column 4 with column 5 = 0.96, root-mean-square error = 0.85 hPa), indicating that the trends of airflow in or out of the tropics are much smaller than the tropical mean SLP trends would suggest. But with an average of 0.05 hPa (100 yr)$^{-1}$ the multimodel mean has nearly no change for the absolute tropical SLP. These area mean trends of the tropics are removed to get the relative trend pattern. The spatial standard deviation of the relative trend pattern varies between 0.07 and 0.23°C (100 yr)$^{-1}$, with an average of 0.14°C (100 yr)$^{-1}$, for T_{tropos} and between 0.20 and 0.78 hPa (100 yr)$^{-1}$, with an average of 0.37 hPa (100 yr)$^{-1}$, for SLP.

The spatial distribution of nearly all IPCC models shows the same characteristic land–sea contrast pattern in the relative T_{tropos} and SLP trends (for some models they are shown in Fig. 8). The question arises as to whether the strength of the land–sea contrast in SLP trends in the individual model depends on the strength of land–sea contrast in T_{tropos} trends. In Fig. 7 the land–sea contrasts in T_{tropos} and SLP are compared against each other. For T_{tropos} the land–sea contrast is defined as the ratio between the absolute land and ocean mean warming trend [as defined in Sutton et al. (2007) for surface temperature]. We can first of all note that the land–sea contrast of T_{tropos} is an order of magnitude smaller than the land–sea contrast of T_{surf} (e.g., in Sutton et al. 2007), which is due to much stronger horizontal diffusion in the free atmosphere. For the land–sea contrast in SLP trends we need a different definition, because the definition as ratio between land and ocean SLP trend would not fit here since the absolute trends are positive and negative. We therefore define the land–sea contrast for SLP trends on the basis of the difference between the average ocean and land trends, with ocean weighted with 80% and land with 20% according to their relative fractions in the tropics. Thus, large deviations from zero indicate a strong land–sea contrast, as spatially independent distributed trends would yield a value of zero. In this figure we can see that the models with a strong land–sea contrast in T_{tropos} tend to have also a strong land–sea contrast in SLP, which is also indicated by the regression line in black, and shows with a $R^2 = 0.66$ a significant relation.

We can take a closer look at the T_{tropos} and SLP trends in some models to get an idea of the extent to which the relationship between T_{tropos} and SLP varies. Figure 8 shows the relative trend pattern and regressions of four models, which cover a wide range of different relationships between T_{tropos} and SLP trends.

The Bjerknes Centre for Climate Research (BCCR) Bergen Climate Model version 2 (BCM2.0) has the weakest land–sea contrast in T_{tropos} and a weak sea–land contrast in SLP (see Fig. 7, number 1), which can be also seen in the trend pattern in Fig. 8a: The strongest warming takes place over the Pacific Ocean and the Atlantic Ocean and the SLP trends are mostly the opposite (pattern correlation = -0.74). Thus, despite the weak land–sea contrast in T_{tropos}, the linear relation between T_{tropos} and SLP is still strong (Fig. 8b, $R^2 = 0.55$). The regression of ocean only (blue line) and land only (red line) grid points yields similar regression coefficients but a higher R^2 value for ocean only and a lower for land only. Furthermore, the land–sea contrast at the surface is 1.35, in the normal range (not shown), but the land–sea contrast in T_{tropos} is 1.01 (Fig. 7), which is very low, indicating that the coupling between surface and troposphere is different than in the other models.

TABLE 1. Some statistical values of all IPCC models investigated in this study; boldfaced last row is the average over all 23 individual models.

Model	Absolute T_{tropos} trend [K (100 yr)$^{-1}$]	Relative T_{tropos} trend [K (100 yr)$^{-1}$]*	Absolute SLP trend tropics [hPa (100 yr)$^{-1}$]	Absolute SLP trend global [hPa (100 yr)$^{-1}$]	Relative SLP trend [hPa (100 yr)$^{-1}$]*	Pattern corr**	Statistical regression-coef (hPa K^{-1})**	R^2 value of statistical regression**	R^2 value of simple physical model**
Multimodel ensemble	3.6	0.10	0.05	−0.10	0.22	−0.90	−2.0	0.82	0.80
BCCR-BCM 2.0	3.1	0.08	0.40	0.27	0.25	−0.74	−2.4	0.55	0.51
CGCM3.1(T63)	4.2	0.12	−0.24	−0.34	0.30	−0.79	−2.0	0.62	0.61
CGCM3.1(T47)	3.7	0.11	−0.16	−0.29	0.28	−0.85	−2.1	0.71	0.69
CNRM-CM3	3.8	0.12	0.45	0.28	0.32	−0.81	−2.2	0.65	0.62
CSIRO-Mk3.0	2.6	0.11	−0.12	−0.20	0.23	−0.70	−1.4	0.50	0.48
CSIRO-Mk3.5	4.0	0.17	−0.26	−0.30	0.47	−0.88	−2.4	0.77	0.70
GFDL-CM2.0	3.8	0.15	−0.16	−0.33	0.36	−0.94	−2.2	0.88	0.84
GFDL-CM2.1	3.8	0.14	0.34	0.18	0.34	−0.85	−2.0	0.72	0.70
GISS-AOM	2.9	0.10	0.17	0.18	0.24	−0.79	−1.9	0.62	0.62
GISS-EH	3.2	0.14	0.08	−0.24	0.37	−0.92	−2.4	0.84	0.76
GISS-ER	3.2	0.13	0.06	−0.27	0.36	−0.91	−2.5	0.83	0.74
IAP-FGOALS1.0	2.8	0.11	0.11	−0.17	0.21	−0.75	−1.5	0.57	0.56
INGV-SXG	3.3	0.12	0.01	−0.18	0.78	−0.28	−1.8	0.08	0.08
INM-CM3.0	3.0	0.12	−0.26	−0.29	0.31	−0.93	−2.4	0.86	0.79
IPSL-CM4	4.2	0.14	−0.13	−0.37	0.34	−0.83	−2.0	0.70	0.68
MIROC3.2(hires)	5.5	0.20	0.53	0.43	0.53	−0.70	−1.9	0.50	0.49
MIROC3.2(medres)	4.1	0.21	0.43	0.30	0.53	−0.88	−2.3	0.78	0.73
MPI-ECHAM5	4.6	0.15	−0.03	−0.22	0.40	−0.65	−1.8	0.42	0.42
MRI-CGCM2.3.2	3.0	0.11	−0.02	−0.16	0.28	−0.76	−2.0	0.59	0.57
NCAR CCSM3	3.2	0.14	0.33	0.25	0.29	−0.77	−1.6	0.59	0.58
NCAR PCM	2.2	0.07	0.21	0.04	0.20	−0.92	−2.4	0.84	0.76
UKMO-HadCM3	3.6	0.23	−0.74	−0.88	0.62	−0.96	−2.6	0.92	0.81
UKMO-HadGEM1	3.9	0.17	0.23	0.01	0.45	−0.89	−2.3	0.80	0.74
Average	**3.6**	**0.14**	**0.05**	**−0.10**	**0.37**	**−0.80**	**−2.1**	**0.67**	**0.63**

* Spatial standard deviation of the relative trend pattern.

** For the two relative trend pattern of SLP and T_{tropos}.

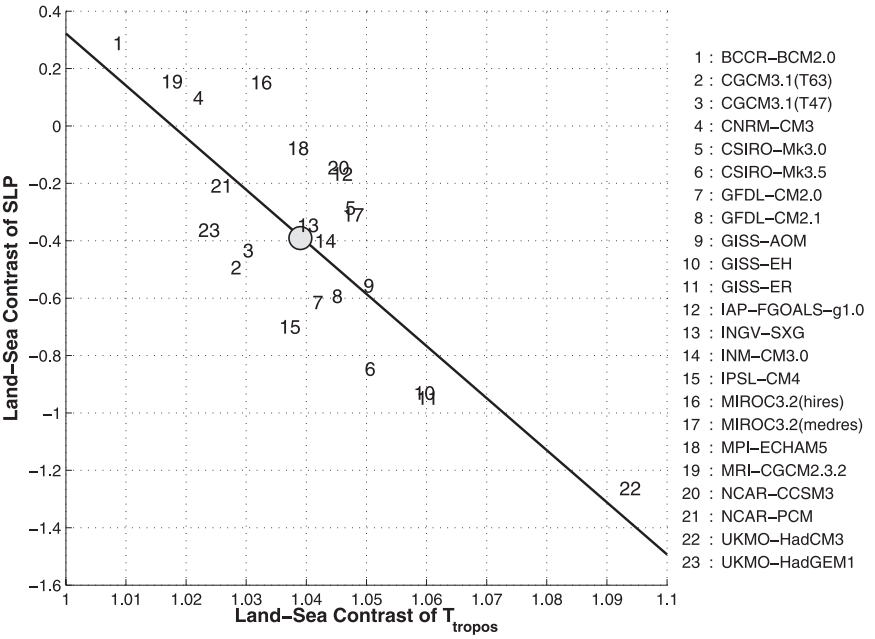

FIG. 7. Land–sea contrast in the individual IPCC models and the multimodel ensemble (circle) for T_{tropos} on the x axis and SLP on the y axis; for the definition of the land–sea contrast see text; the black line is the regression line with $R^2 = 0.66$.

The Max-Planck Institute (MPI) ECHAM5 model has virtually no land–sea contrast in SLP and is in the lower middle of the land–sea contrast range of T_{tropos} (see Fig. 7, number 18); even so, the land–sea contrast is clearly imposed on both trend patterns in Fig. 8c. The SLP trends disagree strongly with our hypothesis above the mountainous regions. The regression (Fig. 8d) shows a relation between these two patterns ($R^2 = 0.42$) and the ocean and land grid points are mostly separated, but not directly along the regression line. The regression for the ocean only and land only grid points has a similar regression coefficient, but a higher R^2 value for ocean only and an even weaker for land only. Here the land–sea contrast values of T_{surf} and T_{tropos} are both in the normal range, but the land–sea contrast in SLP is very low (Fig. 7), so that in this model the coupling of T_{tropos} and SLP over the mountainous regions seems to be different from the other models.

The Geophysical Fluid Dynamics Laboratory Climate Model version 2.1 (GFDL CM2.1) model is in the upper middle of the land–sea contrast range (see Fig. 7, number 8) and the trend pattern (Fig. 8e) looks quite similar to those of the multimodel ensemble. The land and ocean points are well separated along the regression line, which show, with $R^2 = 0.72$, a strong relation (Fig. 8f). The regression for ocean only and land only is here quite similar to the all-grid-points regression.

The third climate configuration of the Met Office Unified Model (HadCM3) is the model with the strongest land–sea contrast (see Fig. 7, number 22) and in the trend patterns (Fig. 8g) the land–sea contrast is imposed on both trend pattern and the amplitudes are stronger than in the multimodel ensemble. The regression (Fig. 8h) shows a clear relation between these two patterns ($R^2 = 0.92$) and a clear separation of ocean and land grid points due to the strong land–sea contrast. Here again the regression for ocean only and land only is quite similar to the all-grid-points regression. In these four models the R^2 value is higher over ocean than over land, with bigger differences in the models where we have only a weak land–sea contrast in T_{tropos} or SLP, so that the interaction over land seems to be the critical point in these models.

Most of the remaining models have trend pattern that are quite similar to the ones of the multimodel ensemble. With pattern correlations between the two trend patterns between -0.28 and -0.96, with an average of -0.80 (Table 1), we can see that in most of the IPCC models the SLP trends are strongly related to the T_{tropos} trends. The statistical regression of the trend patterns yields values between -1.4 and -2.6 hPa K^{-1} (Fig. 9), with an average of -2.1 hPa K^{-1}, and R^2 values between 0.08 and 0.92, with an average of 0.67. These regression coefficients are on average again a bit stronger than in the simple physical model (black dashed line),

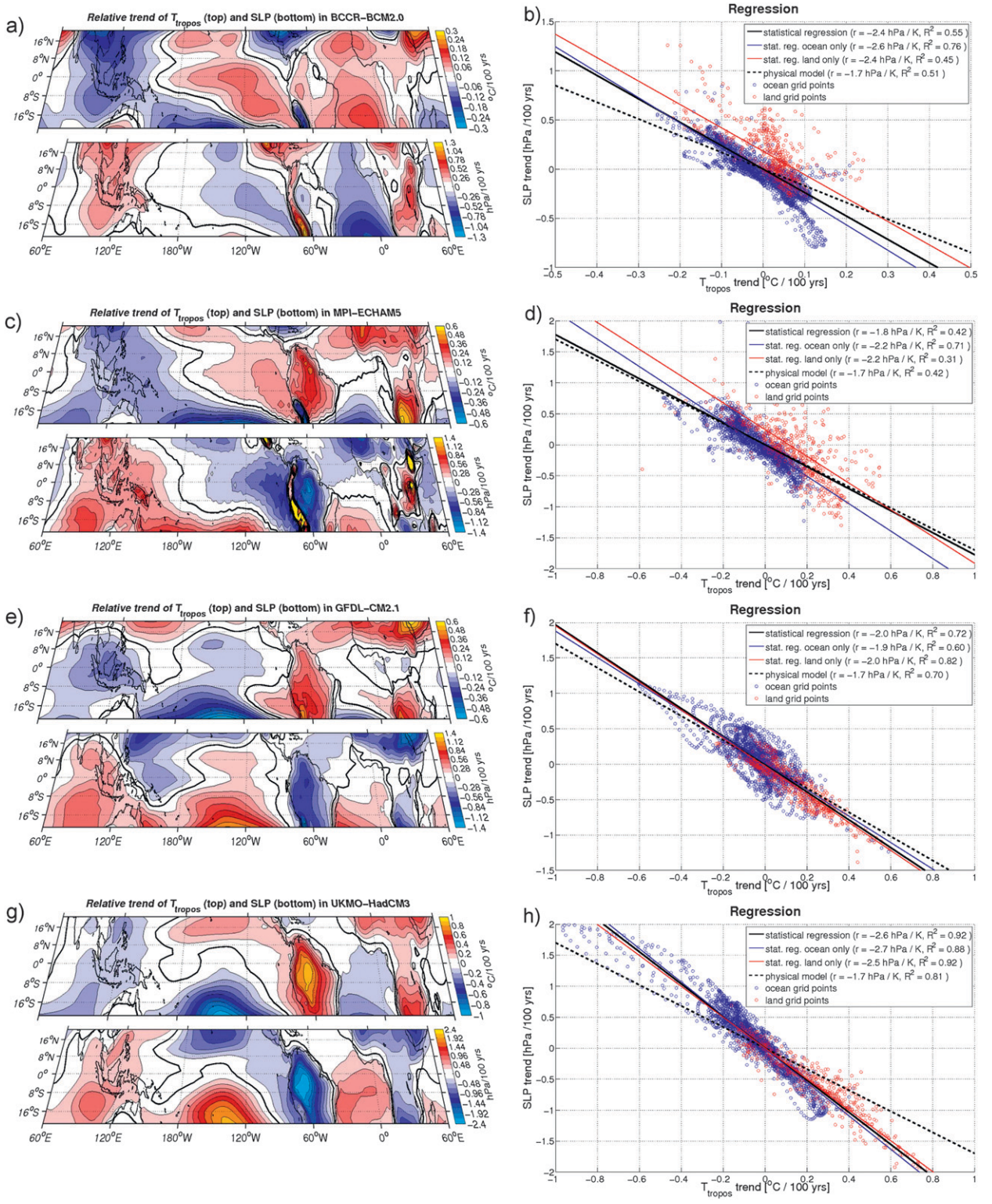

FIG. 8. As in Figs. 5a,b, but for (a),(b) BCCR BCM2.0; (c),(d) MPI ECHAM5; (e),(f) GFDL CM2.1; and (g),(h) HadCM3.

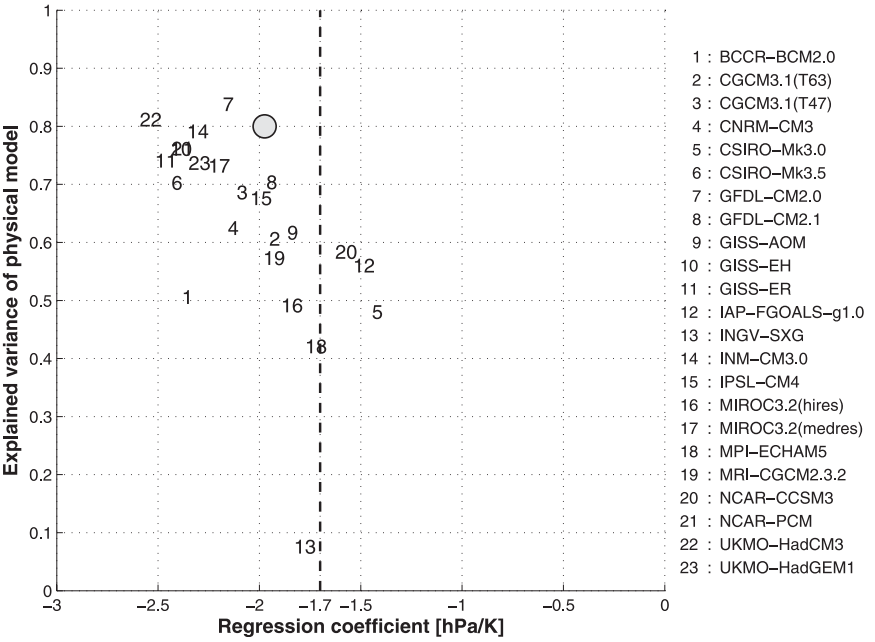

FIG. 9. Comparison of regression coefficient and explained variance of the physical model in the individual IPCC models and the multimodel ensemble (circle). The black dashed line represents the corresponding sensitivity coefficient of the physical model.

indicating that the simple model underestimates the link between T_{tropos} and SLP. The simple model can explain in the individual IPCC models between 8% and 84% of the SLP trends, with an average of 63%, but with all except one model explaining more than 40% (Fig. 9).

We conclude that the strong coupling between the T_{tropos} and SLP trends is evident in most of the models, even if the land–sea contrast is not the dominant signal in the trends, as in BCCR CM2.0 model. And models that have a strong land–sea contrast in T_{tropos} trends tend to have also a strong land–sea contrast in SLP trends. Furthermore, in most of the models the land–sea contrast is the dominant signal in the trend pattern. As stated in the introduction, the land–sea contrast depends on available moisture, so that we expect a stronger warming in T_{tropos} and decreasing SLP over the South American/African sector and a relative cooling in T_{tropos} and increasing SLP over the Indo-Pacific warm pool region. This is true for nearly all individual models with a strong linear relation (Fig. 10).

7. SLP response in idealized T_{land} + 1 K experiment

We can use a set of atmospheric general circulation model (AGCM) experiments to investigate how the atmospheric circulation responds to tropical land warming. This should give some support for the hypothesis that the SLP trends are primarily a response to the tropospheric temperature warming pattern, which is dominated by the land–sea warming contrast. We therefore analyze some experiments of Dommenget (2009), in which the response of an AGCM to warming of the global land by +1 K and cooling of the global land by −1 K is simulated. The SST in the AGCM is free to respond, as the SST is simulated by a simple single column ocean mixed layer model; see Dommenget (2009) for details. Thus, these experiments are not constructed in a way that they can exactly reproduce the IPCC runs, as the surface land warming is here prescribed homogeneously over all land points, independent of available moisture or distance to the coasts.

The results are shown in Fig. 11, with the response defined as the difference between the land +1 K minus the land −1 K divided by 2. The ocean warms much less than 1 K in response to the 1-K surface land temperature increase (Fig. 11a), as discussed in Dommenget (2009), and surface temperature has a very strong land–sea contrast of 5.1. The relative response of tropospheric temperature is positive over the continents and mostly negative over the oceans, with higher response over the dry subtropics than over the wetter tropics (Fig. 11c, top), as expected from the land–sea warming contrast. In agreement with the Bjerknes circulation theorem the SLP response is mostly the opposite of the T_{tropos} response (Fig. 11c, bottom; pattern correlation −0.89).

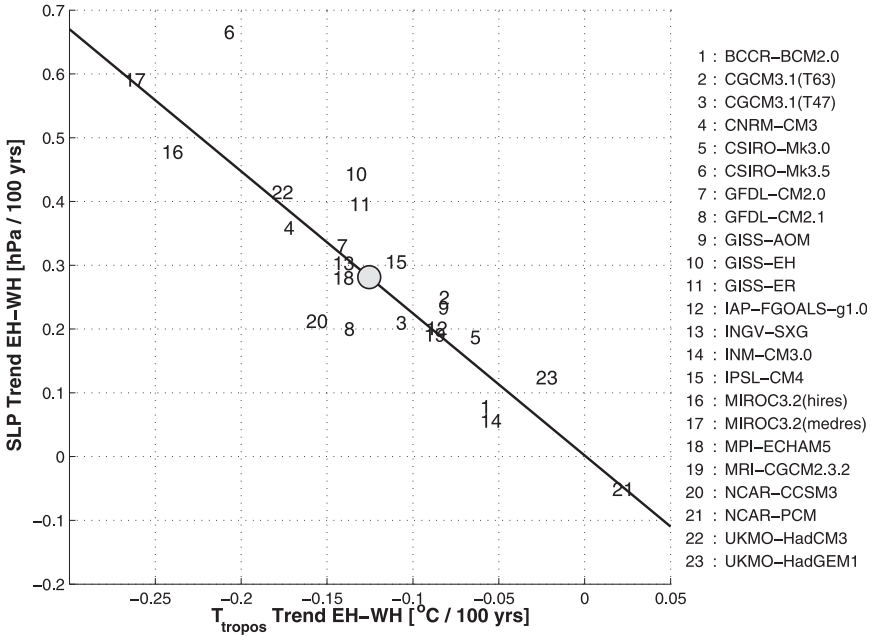

FIG. 10. Comparison of the "eastern" hemispheric (23°S–23°N, 60°E–120°W) minus the "western" hemispheric (23°S–23°N, 120°W–60°E) trend of T_{tropos} (on the x axis) and SLP (on the y axis) of the individual IPCC models and the multimodel ensemble (circle); the black line is the regression line with $R^2 = 0.79$.

These patterns have similar trends to the global warming runs over Africa, the Atlantic, South America, and the Pacific, but disagree in sign over Southeast Asia, the Maritime Continent, and Australia. In the idealized runs we have a clear land–sea contrast signal over the warm pool region, as they are prescribed, but in the IPCC runs there is no land–sea contrast in T_{tropos} and SLP. As stated above, this difference can be explained with the experimental setup of the idealized experiments, where the land–sea contrast is forced by the fixed land surface temperature change.

A regression between these two response patterns yields a regression coefficient similar to the sensitivity coefficient of the physical model (2.0 hPa K^{-1}; Fig. 11b)

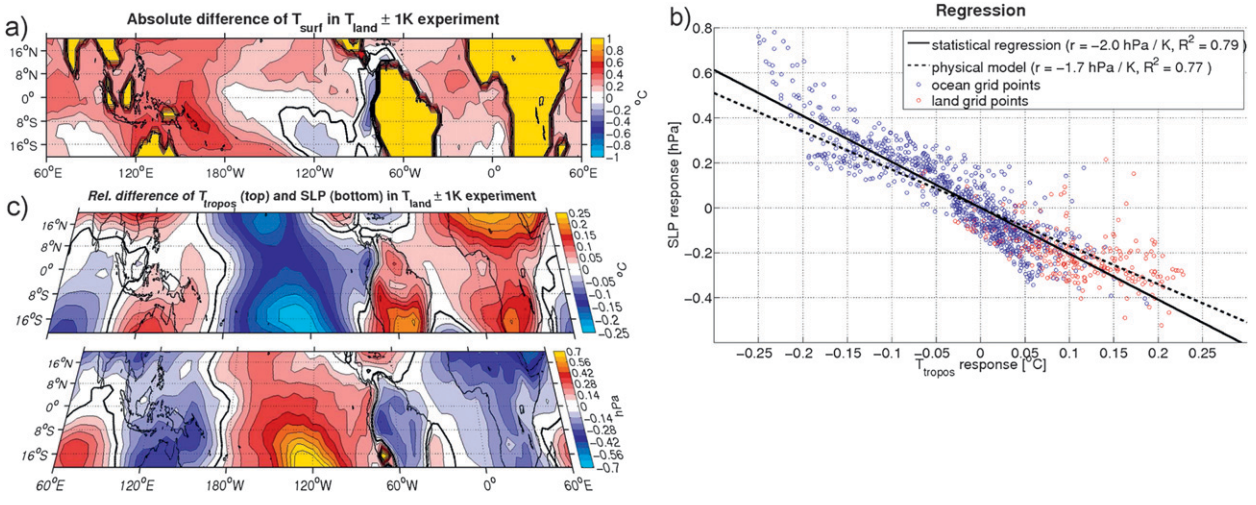

FIG. 11. (a) Absolute difference of T_{surf} in the idealized T_{land} ±1 K experiment. (b),(c) As in Figs. 5a,b, but showing the relative difference of the idealized experiment, with area mean response of 0.6°C for T_{tropos} and −0.05 hPa for SLP removed; pattern correlation = −0.89.

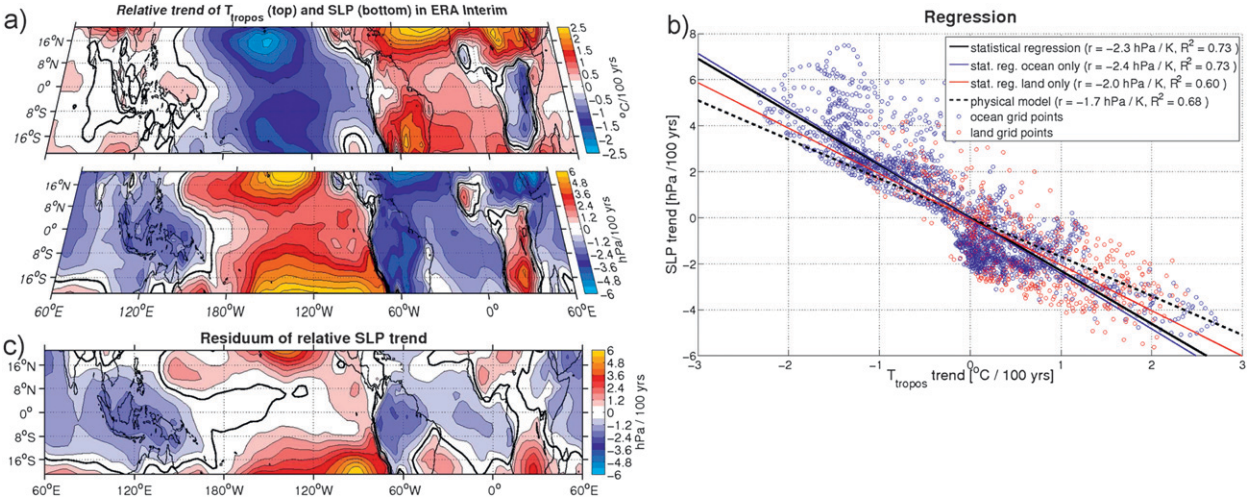

FIG. 12. As in Fig. 5, but for the ERA-Interim reanalysis data in the period 1989– 2010, with the area mean trend removed in (a): 1.7°C (100 yr)$^{-1}$ for T_{tropos} and −1.2 hPa (100 yr)$^{-1}$ for SLP.

and 79% of the SLP response can be explained by the T_{tropos} response in a linear fit (77% in the physical model). The ocean and land grid points are clearly separated along the regression line, indicating that the land–sea contrast is the major forcing in this two-trend pattern. In summary, in these idealized experiments the trend patterns support our hypothesis, that land–sea contrast is the major driver for the large-scale SLP response in a warming climate.

8. Observed trends in ERA-Interim

We can now look at observed trends in the tropics over the last two decades to see if a strong relation between relative T_{tropos} and SLP trends exists there too. However, we have to keep in mind a few important differences between the observed and simulated trends: first, the observed trends are more uncertain than those of the IPCC scenario simulations, due to the much shorter observed time period of 22 years versus the 130 years of the IPCC scenario simulations used to estimate the trends. Second, it has to be noted that the trends in the twentieth century are weaker than those of the twenty-first century, which will lead to a weaker trend signal in the observation compared to the IPCC scenario simulations. Third, it should be noted that tropical natural variability, such as El Niño, has a stronger impact on relative short time period trends, which will decrease the signal-to-noise ratio in the observations. Finally, we have to consider that the observations are just one realization of the warming trend, whereas the IPCC scenario simulations are 23 realizations averaged to one ensemble mean. Thus, the observed trends will be much more uncertain and will contain a much larger fraction of internal natural variability than the IPCC scenario simulations.

The trend patterns for the period 1989–2010 shown in Fig. 12a have some similarities with the projected trend pattern of the IPCC models, but the amplitudes over ocean are larger than those over land. The overall T_{tropos} warming trend of 1.7°C (100 yr)$^{-1}$ lies within the range of trends due to natural variability simulated by a control simulation of a coupled ECHAM5 model (Bengtsson and Hodges 2009). Again, these two patterns are highly anticorrelated (−0.85) and pattern regression yields a regression coefficient of −2.3 hPa K^{-1} (Fig. 12b). In the point clouds, the land and ocean grid points are only weakly separated, indicating that land–sea contrast is not dominating this trend pattern. The regression for ocean only (blue line) and land only (red line) yields similar values as for all grid points, with a slightly smaller regression coefficient and R^2 value for land only. The large-scale residuum pattern obtained from the simple model (Fig. 12c) has a quite similar structure to the trend pattern, but weaker amplitudes. The physical model can explain 68% of the SLP trends.

9. Summary and discussion

In the study presented above we address the causes of the large-scale tropical SLP changes during climate change. Since tropical SLP is an important indicator for the mean state and variability of the tropical atmospheric circulation we implicitly assume that the analysis of the tropical SLP changes will provide us a basis for understanding changes in the tropical

atmospheric circulation. The analysis we present was based on the CMIP3 climate model simulations for future climate change scenarios, the observed seasonal cycle, and recent observations of trends in the tropical climate.

In summary, we found a quite robust and strong relationship between the large-scale trends in tropical T_{tropos} and SLP. This relationship is physically based on the thermodynamic response of the SLP to inhomogeneous T_{tropos} warming. In this picture, the trends in the T_{tropos} warming drive the large-scale changes in SLP. This is evident in nearly all IPCC models, independent of whether the land–sea contrast dominates the two-trend pattern or not. With the help of a simple physical model, we can measure the ratio between the SLP and T_{tropos} trends (-1.7 hPa K^{-1}) and can predict a large part of the SLP trends if we know the T_{tropos} trends. Furthermore, the dominant feature of the inhomogeneous T_{tropos} warming, which is in most of the IPCC simulations the land–sea contrast, is imprinted onto the SLP trend pattern as well. This leads to decreased SLP over South America, the Atlantic, and parts of Africa and increased SLP over the tropical Indo-Pacific warm pool and implies changes in the regional distribution of tropical deep convection. Indeed, all of the IPCC models except one predict increasing SLP and a weaker warming of T_{tropos} over the warm pool region and decreasing SLP and a stronger warming of T_{tropos} over the South American/African region (Fig. 10).

In the comparison of the IPCC models it becomes evident that the models that have a strong land–sea contrast in T_{tropos} tend to have also a strong land–sea contrast in SLP. Furthermore, we could support our hypothesis with an idealized sensitivity experiment, in which we prescribed the land warming.

In recent years the tropical SLP response in global warming was often discussed in the context of the enhanced hydrological cycle and the accompanied weakening of the tropical circulations, as in Vecchi and Soden (2007, hereafter VS07). This discussion, however, did not consider the second important change of tropical temperature: the land–sea warming contrast. The question arises: How does our new idea fit in their discussion about the weakening Walker circulation? VS07's Fig. 10 (top) is similar to our Fig. 5a (bottom) with a similar tendency in the relative SLP trends over the Indo-Pacific warm pool region and the tropical Pacific, even though they only considered SLP changes only over the oceans. VS07 based their argument on the interaction between SST in this region and the Walker circulation, but they found a disagreement between the SLP and SST change. Further, it needs to be noted that our simple model does not make any statement on how the tropical Pacific SST may change, which is central to the VS07 study. The simple model discussed here explains a large fraction of the total SLP trends over the Indo-Pacific warm pool region ($R^2 = 0.81$), but the residuum of this model still shows a decrease in SLP gradient over the Pacific Ocean that would fit the VS07 study. In turn, our explanation for the roughly zonal SLP response due to inhomogeneous T_{tropos} warming could be the missing piece, explaining why the zonal Walker circulation weakens stronger than the meridional Hadley circulation. Two of the three main convection regions (South America and Africa) warm more strongly than the third (the Indo-Pacific warm pool), which decreases the relative importance of the latter. This zonal inhomogeneous distribution of the land–sea contrast leads to zonal changes that affect the Walker circulation but do not affect the Hadley circulation that much. Thus, it seems that both approaches fit together: VS07 considering the changes in the vertical temperature profile and this study the horizontal ones. However, the results presented here suggest that land–sea warming contrast is probably the most important driver of the large-scale SLP change and that future changes in the spatial distribution of relative low SLP, with associated upward air motion, which would favor deep convection conditions, are strongly controlled by the relative changes in tropospheric temperatures.

From reanalysis data the question arises if the trend in the tropical SLP is the warming climate signal as seen in the IPCC simulations or if it is natural variability. The trend patterns show some similarities to those in the IPCC simulations, but this trend lies within the range of natural variability, simulated by a control simulation of a coupled ECHAM5 model (Bengtsson and Hodges 2009) and both variables have stronger trends over oceans than over land. Furthermore, the negative SLP trend over the Maritime Continent together with the positive trend over the east Pacific shows an increase in the zonal SLP gradient over the Pacific, which can be interpreted as an increase in strength of the Walker circulation due to natural variability, as proposed by Meng et al. (2012). The response of the equatorial Pacific in a warming climate is a topic of recent research (e.g., DiNezio et al. 2009; Park et al. 2009) but still model dependent (Latif and Keenlyside 2009). From these uncertainties in the dynamical response and the short records of observations it is difficult to assess what part of the observed trends is natural variability and what is climate change. However, the relative trends of T_{tropos} and SLP in observations are also strongly related, following mostly the simple thermodynamical model discussed in this study.

Acknowledgments. We acknowledge the individual modeling groups, the Climate Model Intercomparison Project (CMIP3), and ECMWF for providing the data sets. This work was supported by the Deutsche Forschungsgemeinschaft (DFG) through project DO1038/5-1 and the ARC Centre of Excellence in Climate System Science (CE110001028). We thank Richard Greatbatch, Jan Harlaß, Kevin Hodges, Noel Keenlyside, Joe Kidston, Mojib Latif, Willi Rath, Thomas Reichler, and the anonymous reviewers for discussion and useful comments.

REFERENCES

Bala, G., K. Caldeira, R. Nemani, L. Cao, G. Ban-Weiss, and H.-J. Shin, 2011: Albedo enhancement of marine clouds to counteract global warming: Impacts on the hydrological cycle. *Climate Dyn.,* **37,** 915–931.

Bengtsson, L., and K. I. Hodges, 2009: On the evaluation of temperature trends in the tropical troposphere. *Climate Dyn.,* **36,** 419–430, doi:10.1007/s00382-009-0680-y.

Bjerknes, V., R. Rubenson, and A. Lindstedt, 1898: Über einen Hydrodynamischen Fundamentalsatz und seine Anwendung besonders auf die Mechanik der Atmosphäre und des Weltmeeres. *Kongl. Sven. Vetenskaps Acad. Handl.,* **31,** 1–35.

DiNezio, P. N., A. C. Clement, G. A. Vecchi, B. J. Soden, B. P. Kirtman, and S.-K. Lee, 2009: Climate response of the equatorial Pacific to global warming. *J. Climate,* **22,** 4873–4892.

Dommenget, D., 2009: The ocean's role in continental climate variability and change. *J. Climate,* **22,** 4939–4952.

——, and J. Flöter, 2011: Conceptual understanding of climate change with a globally resolved energy balance model. *Climate Dyn.,* **37,** 2143–2165, doi:10.1007/s00382-011-1026-0.

Flohn, H., 1975: Tropische Zirkulationsformen im Lichte der Satellitenaufnahmen. *Bonner Meteor. Abhandl.,* **21,** 1–82.

Gill, A. E., 1980: Some simple solutions for heat-induced tropical circulation. *Quart. J. Roy. Meteor. Soc.,* **106,** 447–462, doi:10.1002/qj.49710644905.

Held, I. M., 1993: Large-scale dynamics and global warming. *Bull. Amer. Meteor. Soc.,* **74,** 228–241.

——, and B. J. Soden, 2006: Robust responses of the hydrological cycle to global warming. *J. Climate,* **19,** 5686–5699.

Hu, Z., M. Latif, and E. Roeckner, 2000: Intensified Asian summer monsoon and its variability in a coupled model forced by increasing greenhouse gas concentrations. *Geophys. Res. Lett.,* **27,** 2681–2684.

Joshi, M. M., J. M. Gregory, M. J. Webb, D. M. H. Sexton, and T. C. Johns, 2008: Mechanisms for the land/sea warming contrast exhibited by simulations of climate change. *Climate Dyn.,* **30,** 455–465, doi:10.1007/s00382-007-0306-1.

Krueger, A. F., and J. S. Winston, 1974: A comparison of the flow over the tropics during two contrasting circulation regimes. *J. Atmos. Sci.,* **31,** 358–370.

Latif, M., and N. S. Keenlyside, 2009: El Niño/Southern Oscillation response to global warming. *Proc. Natl. Acad. Sci. USA,* **106,** 20 578–20 583.

Matsuno, T., 1966: Quasi-geostrophic motions in the equatorial area. *J. Meteor. Soc. Japan,* **44,** 25–43.

Meehl, G. A., and Coauthors, 2007a: Global climate projections. *Climate Change 2007: The Physical Science Basis,* S. Solomon et al., Eds., Cambridge University Press, 747–846.

——, C. Covey, T. Delworth, M. Latif, B. McAvaney, J. F. B. Mitchell, R. J. Stouffer, and K. E. Taylor, 2007b: THE WCRP CMIP3 multimodel dataset: A new era in climate change research. *Bull. Amer. Meteor. Soc.,* **88,** 1383–1394.

Meng, Q., M. Latif, W. Park, N. S. Keenlyside, V. A. Semenov, and T. Martin, 2012: Twentieth century Walker circulation change: Data analysis and model experiments. *Climate Dyn.,* **38,** 1757–1773, doi:10.1007/s00382-011-1047-8.

Park, W., N. S. Keenlyside, M. Latif, A. Ströh, R. Redler, E. Roeckner, and G. Madec, 2009: Tropical Pacific climate and its response to global warming in the Kiel climate model. *J. Climate,* **22,** 71–92.

Roeckner, E., and Coauthors, 2003: The atmospheric general circulation model ECHAM5. Part I: Model description. Max Planck Institute for Meteorology Rep. 349, 127 pp.

Simmons, A., S. Uppala, D. Dee, and S. Kobayashi, 2007: ERA-Interim: New ECMWF reanalysis products from 1989 onwards. *ECMWF Newsletter,* No. 110, ECMWF, Reading, United Kingdom, 25–35.

Sutton, R. T., B. Dong, and J. M. Gregory, 2007: Land/sea warming ratio in response to climate change: IPCC AR4 model results and comparison with observations. *Geophys. Res. Lett.,* **34,** L02701, doi:10.1029/2006GL028164.

Thorpe, A. J., H. Volkert, and M. Ziemianski, 2003: The Bjerknes circulation theorem: A historical perspective. *Bull. Amer. Meteor. Soc.,* **84,** 471–480.

Vecchi, G. A., and B. J. Soden, 2007: Global warming and the weakening of the tropical circulation. *J. Climate,* **20,** 4316–4340.

——, ——, A. T. Wittenberg, I. M. Held, A. Leetmaa, and M. J. Harrison, 2006: Weakening of tropical Pacific atmospheric circulation due to anthropogenic forcing. *Nature,* **441,** 73–76, doi:10.1038/nature04744.

——, A. Clement, and B. J. Soden, 2008: Examining the tropical Pacific's response to global warming. *Eos, Trans. Amer. Geophys. Union,* **89,** 81, doi:10.1029/2008EO090002.